RUSSIAN JOURNAL OF EARTH SCIENCES, VOL. 12, ES2003, doi:10.2205/2011ES000507, 2011

# Sample application of a low-cost X-band monitoring system of surface currents at the Black Sea shore

D. V. Ivonin[1], V. A. Telegin[2], V. V. Bakhanov[3], A. V. Ermoshkin[3], and A. I. Azarov[4]

Received 5 July 2011; accepted 24 August 2011; published 30 September 2011.

Nautical X-band radar (low-cost option with the antenna beamwidth 1.9°) was applied for monitoring surface near-shore currents in the Black Sea Field Research Facility of the Southern Branch of P. P. Shirshov Institute of Oceanology. The radar signal was processed by an algorithm based on the Nieto-Borge approach. The experimental setup is shown to allow precise real-time near-surface current measurements up to 4 km offshore. A case study of a coherent current pattern resembling a sub-mesoscale vortex passing the experimental field is presented. *KEYWORDS: X-band radar; radiowave oceanography; currents; sub-mesoscale vortex; Black Sea.*

**Citation:** Ivonin, D. V., V. A. Telegin, V. V. Bakhanov, A. V. Ermoshkin, and A. I. Azarov (2011), Sample application of a low-cost X-band monitoring system of surface currents at the Black Sea shore, *Russ. J. Earth. Sci., 12,* ES2003, doi:10.2205/2011ES000507.

## Introduction

Remote sensing methods become a powerful tool of research and monitoring sea state, especially, in the near-shore zone. This paper opens a series of reports on current works in the Black Sea Field Research Facility of the P. P. Shirshov Institute of Oceanology of Russian Academy of Sciences (FRF IORAS). These works are motivated by burning problems of developing regular monitoring network for coastal zone of the Black Sea. Developing new radiophysical methods, methods of data processing and assimilation, studies of a variety of hydrophysical, chemical and biological processes are important directions of the interdisciplinary works. The Black Sea Field Research Facility of the P. P. Shirshov Institute of Oceanology is seen as a natural laboratory for elaborating the new approaches for their further dissemination and adaptation in industry, ecology and education.

Nautical no-coherent X-band radars (frequency $\sim 10$ GHz) are used for measurements of the sea state and the surface currents since the 90-th of the last century [*Nieto Borge et al.,* 1999; *Reichert et al.,* 1999]. The commercial radar systems WaMos II and SeaDarQ were developed on their base [*Groeneweg et al.,* 2011; *Nieto Borge et al.,* 2006; *Reichert et al.,* 1999]. WaMos II developers announced possibility to measure the directional spectrum of sea waves and the surface currents for 2 minutes data accumulation. The minimal radar requirements for such measurements [*Reichert et al.,* 1999] are: 1) the minimal antenna rotation speed is 24 rpm (the antenna rotation time $< 2.5$ s); 2) the maximal radar pulse length is 80 ns; 3) the antenna angular resolution is better then 0.95° (the minimal antenna length is 2.44 m). The system covers the range from 0.1 km to 5 km depending on the wind speed and the installation height. The system performance depends on weather conditions as well: the wind speed should be higher than 3 m $s^{-1}$.

The significant wave height measurements implemented by such radar systems were tested successfully in a number of works by comparison with the buoy and other independent measurements [*Hessner et al.,* 2003; *Nieto Borge et al.,* 1999, 2006; *Reichert et al.,* 1999; *Vogelzang et al.,* 2000]. It should be noted that almost all of the cited radar vs. buoy comparisons have been done very close to the radar site (500–850 m). The only case of larger distance from the radar (2.7 km) is represented by the work [*Hessner et al.,* 2003].

The surface currents measurements are represented relatively poor, in the literature. Generally, cases of extreme tidal current velocities (up to a few meters per second) are discussed [*Groeneweg et al.,* 2011; *Vogelzang et al.,* 2000].

The network developed in FRF IORAS is based on low-cost X-band radars. The latter, of course, have lower operating characteristics then Wamos II and SeaDarQ. The key limitation of low-cost radars is the antenna angular resolution. Some radars can have 5.2° or 1.9° angular resolution

[1]P. P. Shirshov Institute of Oceanology, Russian Academy of Science, Moscow, Russia
[2]Research Institute of Long-Range Radiocommunication, Moscow, Russia
[3]Institute of Applied Physics, Russian Academy of Science, Nizhnij Novgorod, Russia
[4]Southern Branch of the P. P. Shirshov Institute of Oceanology, Russian Academy of Science, Gelendzhik, Krasnodar Region, Russia

**Figure 1.** Radar site during 2008 year experiment.

that is twice or more worse than the recommended value of 0.95°. The results of testing the radar with 1.9° angular resolution are presented in this work. Examples of the surface current measurements got by such radar are shown. The results are shown to be consistent with the satellite images of vortex structures in this region.

The work is organized as follows. In section "Radar" we give the technical specification of the radar and data acquisition system. In section "Method" the brief basics of the physical model of electromagnetic scattering and the associated method of radar data processing are presented. In "Results" we retrieve the radial component of the current velocity. Basing on this scalar velocity field and additional hypotheses we, then, reconstruct a velocity vector field. Satellite images and in situ measurements of a mesoscale vortex found in the experimental site are used for verification this reconstruction. "Discussion" we describe limitations of our experimental setup due to the low antenna angular resolution and the speckle-noise raise. In concluding remarks we summarize the results and discuss the perspectives.

## Radar

The radar Furuno 1832 (X-band, frequency 9.41 GHz) with the antenna beamwidth 1.9° (horizontal) was used in the experiments (see Figure 1). The used pulselength 80 ns provided the radial distance resolution about 12 m. The radar video signal output was connected to the analog-digital converter where the signal was sampled at frequency 25 MHz (that corresponds to the formal distance resolution ≈ 6 meters) and recorded up to distance 6 km. In average, 574 directions were saved for each antenna turn (that corresponds to the formal angular resolution 0.63°). The wind and weather conditions were registered by the portable meteo station Davis Instrument Wantage Pro2.

## Method

The method developed by *Nieto-Borge et al.* [1999] for measurements of sea wave heights and surface currents was applied. The method is based on the assumption that the Bragg backscattering from the gravity-capillary ripples contributes mainly to the signal. The ripples are modulated by longer waves that makes the long wave patterns visible on the radar screen. The method includes the following steps (we give here the brief description of the steps only, the full description can be found in [*Hessner et al.,* 2003; *Nieto Borge et al.,* 1999, 2006; *Reichert et al.,* 1999]):

1. acquisition of a set of radar images for 32 antenna turns (2 min data accumulation);

2. picking on an area of interest of 128 points in radial distance and 32 points in angle (this corresponds to the area 770 × 1050 $m^2$ at distance 3 km from the radar) and converting these data from the polar coordinates to the Cartesian ones to get the data array $T_{3d}(x,y,t)$ of the size (128, 32, 32);

3. 3-d Fourier transform of the data array $T_{3d}(x,y,t)$ to get the three-dimensional spectrum $F_{3d}(k_x, k_y, \omega)$

$$F_{3d}(k_x, k_y, \omega) = \iiint T_{3d}(x, y, t) e^{-ik_x x - ik_y y + i\omega t} dx dy dt \quad (1)$$

where $k_x$ and $k_y$ (in rad m$^{-1}$) are the radial and the tangent components of the wavevector $\mathbf{k}$, $\omega$ is the angular frequency (in rad s$^{-1}$);

4. transformation of 3-d Fourier spectrum $F_{3d}(k_x, k_y, \omega)$ into the two dimensional wavenumber/frequency spectrum $F_{2d}(|k|, \omega)$ in a chosen sector of wave directions

$$F_{2d}(|k|, \omega) = \int\limits_{k=\sqrt{k_x^2+k_y^2}} F_{3d}(k_x, k_y, \omega) dk_x \quad (2)$$

5. suppressing the speckle noise and filtering the signal corresponding to the gravity sea waves;

6. calculation of the velocity of surface currents.

One of the most interesting features of the signal processing is the filtering of the signal corresponding to the gravity sea waves. The key point is that the signal coming from the gravity waves should obey the dispersion relation

$$\omega_w = \sqrt{gk} + k\, U \cos\alpha \quad (3)$$

Here $\omega_w$ (in rad s$^{-1}$) is the angular frequency of the waves, $g = 9.8$ m s$^{-2}$ is the gravity acceleration, $k$ (in rad m$^{-1}$) is the wavenumber ($k = \sqrt{k_x^2 + k_y^2}$), $U$ (in m s$^{-1}$) is the current velocity, $\alpha$ is the angle between wavevector $\mathbf{k} \equiv (k_x, k_y)$ and the current.

The second term in (3) reflects the result of the sea waves interaction with the current. It is possibly to estimate the radial component $U\cos\alpha$ of the current by evaluating the value of this frequency shift from the base value $\sqrt{gk}$. In the case when a wide-angle sea wave spectrum is observed it is possible to reconstruct not only the radial component but the velocity $U$ and the current direction $\alpha$ themselves. The shift value was estimated by minimizing the integral $I(U, \alpha)$ over the filtered part of the two dimensional frequency-wavenumber spectrum $F_{2d}(|k|, \omega)$

$$I(U, \alpha) = \int\limits_{k_{\min}}^{k_{\max}} \int\limits_{\omega_{\min}}^{\omega_{\max}} F_{2d}(|k|, \omega)\, dk\, d\omega \quad (4)$$

where

$$k_{\min} = 0.13 \text{ rad m}^{-1} \quad (5)$$
$$k_{\max} = 0.27 \text{ rad m}^{-1} \quad (6)$$
$$\omega_{\min} = \sqrt{gk} + kU\cos\alpha - 2\pi\Delta f \quad (7)$$
$$\omega_{\max} = \sqrt{gk} + kU\cos\alpha + 2\pi\Delta f \quad (8)$$
$$\Delta f = 0.15 \text{ Hz} \quad (9)$$

# Results

## Data

The experiments were carried out during the short-term works in 2006–2008 years at the Black Sea, near Gelendzhik (44.576° N, 37.977° E). The data corresponding to the wavy sea conditions were selected for processing. The best data were ones registered for the situations when the wind was blowing from the sea to the shore. These are the south and south-west winds. While the north winds happened to be inapplicable for current measurement because the wind could not drive waves sufficient for distinguished backscatter signal up to the distance 4 km from the shore.

The radar was placed inside the bay so the radar sector was limited by close capes from left and right (Figure 1). The data were available in the sector from 150° to 190° counted from the North.

## Wavenumber-Frequency Spectra

The most informative and representative part in the data processing is the analysis of the wavenumber-frequency spectra $F_{2d}(|k|, \omega)$ of the signal. We show two examples of such spectra in Figure 2. They correspond to the distances 1 km and 4 km from the radar and the angle 160° from the North. The south wind 6 m s$^{-1}$ was blowing from the sea toward the shore. On each figure there is pronounced peak placed near the dispersion relation curve marked by the solid blue line. The peak is visible at the wavenumbers 0.13–0.25 rad m$^{-1}$ that correspond to the sea wave lengths from 25 m to 50 m. It can be observed that the peak at the figure corresponding to the distance 1 km is more pronounced then that at the figure for 4 km distance. This effect is due to influence of the raising level of the speckle noise with the distance. This problem will be discussed below in the section deduced to the speckle noise influence on the measurements.

It can be seen in Figure 2a a frequency shift of peak position (marked by the dashed white line). This shift that can be attributed to the current value of 11 cm s$^{-1}$. For comparison, there is no such shift in Figure 2b for 4 km distance. This fact does not mean the absence of the current at the distance 4 km. It means only that the projection of the current velocity vector on the radial direction from the radar is zero. But the current can be directed perpendicular to the radial direction.

## Radial Velocity Field

In the radar sector from 150° to 190° it was possible to get the velocity fields up to the distance 4 km from the radar. To obtain the velocity field we divided the region of radar probing into 20 cells: four through the radius from 1 km to 4 km with the step 1 km, and five through the angle from 150° to 190° with the step 10°. The cell had the size of 700 ×

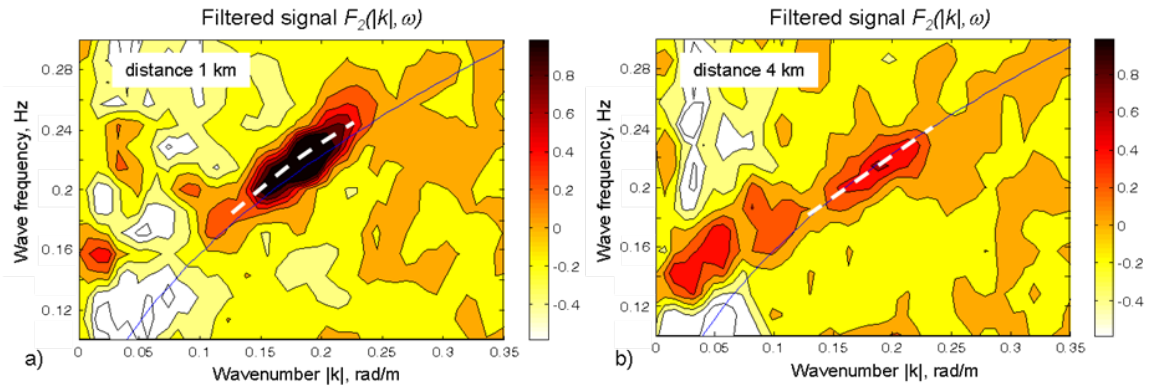


**Figure 2.** The two-dimensional filtered spectrum $F_{2d}(|k|, f)$, 14 September, 2008, wind 6 m s$^{-1}$ SSS. The strong signal corresponding to gravity sea waves is seen in the range $0.13 - 0.24$ rad m$^{-1}$. The dispersion relation (without current) is shown by solid line. The dash line marks the peak position shifted by current.

700 m$^2$ approximately depending on the radial distance. We proceeded the steps 1–6 described in section "Method" for each cell and composed the velocity field.

It should be noted that using the data from the radar with the antenna aperture 1.9° it was possible to obtain only the radial component at distances greater than 2 km. This was caused by the insufficient space resolution (in the tangent direction) at large distances ($> 2$ km) from the radar. So the directional spectrum of the sea surface waves could not be resolved. This resulted in that the various projections of the wavevector **k** on the current direction given by $\cos\alpha$ in the dispersion relation (3) could not be used to evaluate the current direction.

Examples of the fields of the velocity radial component are shown in Figure 3. The first example is for 14 September, 2008, when the south wind of 6 m s$^{-1}$ was blowing (Figure 3a), the second is for 12 September, 2008, when there was the south-west wind of 3–5 m s$^{-1}$ (Figure 3b). It seen in Figure 3a that the radial velocity varies from $-25$ cm s$^{-1}$ to 25 cm s$^{-1}$ with zero value just in the center of the figure while two days before the radial velocity had homogenous character. The radial velocity in Figure 3b varies slightly near 30 cm s$^{-1}$.

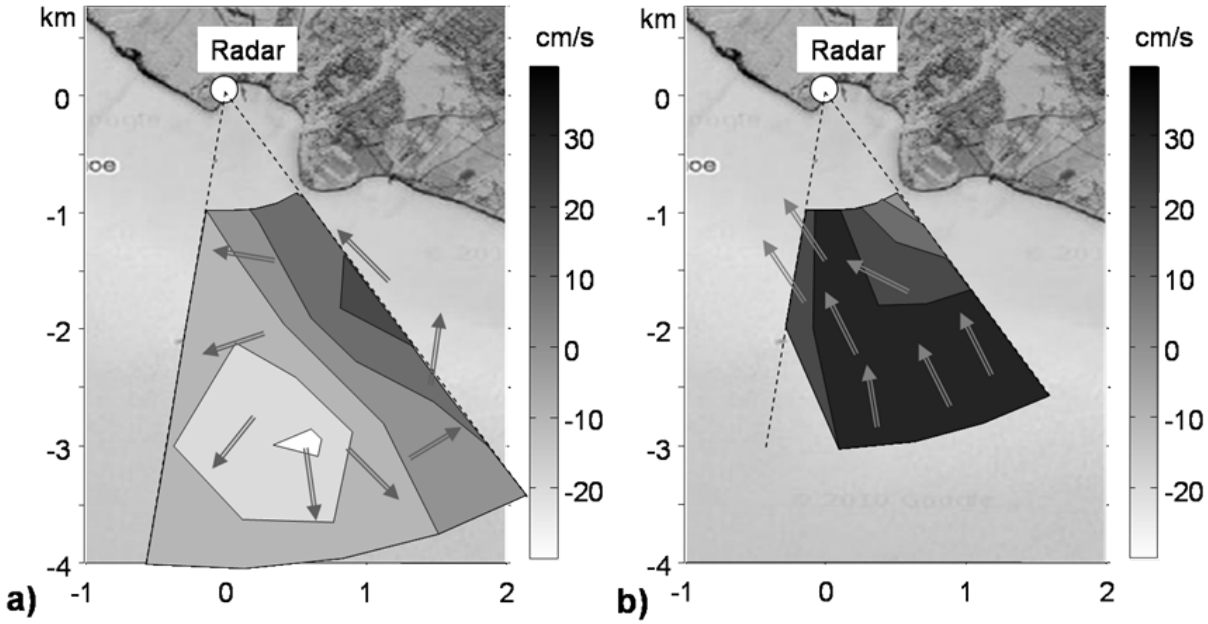


**Figure 3.** The radial component of the current velocity: a) on 14 September, 2008; b) on 12 September, 2008. Arrows mark the behavior of the suggested cyclonic vortex.

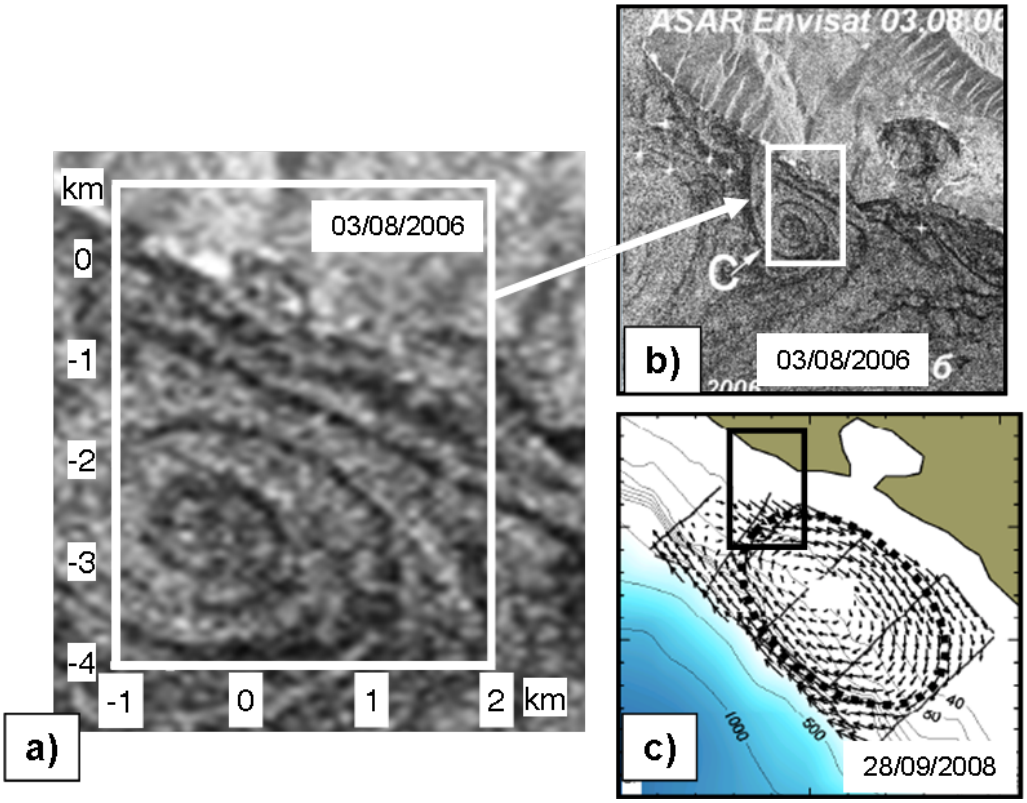


**Figure 4.** a) fragment of ENVISAT image of the region of interest with the cyclonic vortex on 3 August, 2006 (cited from [*Zatsepin et al.,* 2011]), the white rectangle marks the radar coverage zone corresponding to September, 2008; b) full ENVISAT image on 3 August, 2006; c) The observation of the sub-mesoscale vortex by ADCP measurements from the ship board on 28 September, 2008 (cited from [*Zatsepin et al.,* 2011]), the black rectangle marks the radar zone coverage.

**Sub-Mesoscale Vortex**

It can be seen in Figure 3a that the radial velocity varies significantly from 0 cm $s^{-1}$ to 25 cm $s^{-1}$ at the right edge of the picture (direction 150° from the North). At the same time the radial velocity varies from $-25$ cm $s^{-1}$ to 15 cm $s^{-1}$ from 190° to 150° at the 3 km distance. Such behavior of the radial velocity leads to the conclusion that the vector field has a cyclonic vortex structure show by arrows in Figure 3a. The analysis of the radial velocity field two days before (12 September, 2008) does not reveal such vortex structure. The current has homogeneous behavior. We can suggest that the vector velocity was directed along the shore from the south-east to the north-west as shown by arrows in Figure 3b.

Comparison of these two results let us assume that a cyclonic vortex of the size 4 km was passing near the radar site on 14 September, 2008. The drift velocity of the vortex along the shore should be about several kilometers per day. To illustrate the fact of often appearance of such vortices near the coast we show in Figure 4a and Figure 4b the Envisat image of a similar cyclonic vortex passing near the radar site. This image was registered in August 3, 2006 by means of the Advanced Synthetic Aperture Radar (SAR), operating in C-band frequency range of from 2 GHz to 4 GHz. The visual detection of the vortex by examining the SAR images of the ocean surface is possible due to the interaction of the sea surface waves (capillary ripples and gravity waves) with the currents and, so, modulation of the sea surface waves (registered by SAR) by the currents. For convenience of the comparison, we mark by the white rectangle in Figure 4a the area corresponding to that covered by Figure 3a. It is seen that the sizes of the both vortices shown in Figure 3a and Figure 4a are similar and close to 4 km.

Existing of such sub-mesoscale vortices near the Black Sea shore was proved by *Zatsepin* [2011] in a result of the current velocity measurements from the ship. The measurements were carried out at the same place almost at the same time on 28 September, 2008. These results (courtesy to Zatsepin) are cited in Figure 4c. Here the anticyclonic vortex is shown. The size of the vortex is about 8 km that is twice greater than obtained from our results (for simplicity of comparison we show by the black rectangle in Figure 4c the region corresponding to that covered by Figure 3a).

So-called sub-mesoscale vortices arise due to the interaction of the Main Black Sea Current with the shore. So two vortices, cyclonic and anticyclonic, appear near the shore drifting slowly from the East to the West together with the Main Black Sea Current. These vortices play significant role in the exchange process in the coastal zone providing the

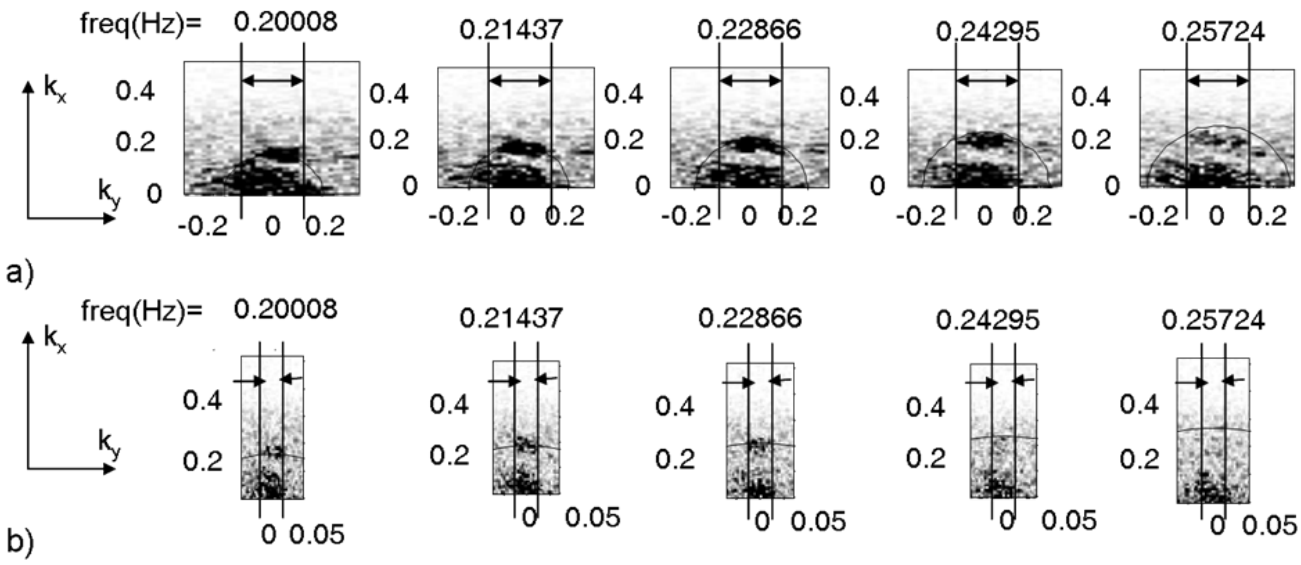


**Figure 5.** Spatial spectra $F_3(k_x, k_y)$ at fixed frequencies (14 September, 2008). a) distance 1 km, b) distance 4 km. The black line marks positions of wave vectors determined from the dispersion relation (3) without currents. The real $k_y$-band resolution is marked by arrows.

delivery of fresh waters from the main bowl of the Black Sea to the coast and removing the dirty waters from the latter.

## Discussion

### Speckle-Noise Influence

The analysis of the radar data revealed very high level of the so-called *speckle noise* in comparison to that observed in the work [*Nieto Borge et al.,* 2006]. So, the signal coming from the sea surface waves was relatively hard to distinguish from the speckle noise. The examples of the speckle noise are shown in Figure 5a, Figure 5b. Here the images of the 3d spectra $F_3(k_x, k_y, \omega)$ at fixed frequencies $\omega$ are shown. The upper picture corresponds to the signal coming from the 1 km distance from the radar. We take the five fixed frequencies from 0.20008 Hz to 0.25724 Hz. These frequencies lay in the wave peak area visible in Figure 2a. The wave signal is distinguished near the circle shown in Figure 5a. This circle marks the possible positions of the wavevector obeying the dispersion relation (3) at chosen frequency $\omega$. The wavenumber $k_x$ corresponds to the radial direction of the radar, $k_y$ corresponds to the tangent direction. The vertical lines with two-sides arrows mark the real radar hardware resolution of the tangent wavenumber $k_y$ (this problem will be discussed in the next subsection deduced to the radar angular resolution).

It is seen in Figure 5a that the signal from the sea waves is weaker than that produced by the speckle noise. The spectrum of the speckle noise $S_n(\mathbf{k})$ in the ideal situation has the form of the Gauss bell-shaped function on $k_x$ and $k_y$ [*Kanevsky,* 2004]

$$S_n(\mathbf{k}) = C_n \exp\left(-ak_x^2 - bk_y^2\right) \tag{10}$$

Here $\mathbf{k} \equiv (k_x, k_y)$, and $a$ and $b$ are some coefficients depending on the radar hardware operating options (radial resolution and angular resolution). So the speckle noise signal has the maximum near zero $k_x$ and $k_y$, and decreases to the periphery wavenumbers. The overall power of the speckle noise is about two orders higher than that of the sea wave signal. This can be seen by comparing the summary area multiplied by the value of the signal taken by the speckle noise and the sea wave signal. (Also, it should be taken into account that there is no wave signal at other frequencies not shown in Figure 5a.)

As a summary of previous paragraph, it is worth to note that only the knowledge about the kinematics and dynamics of the sea surface waves expressed in the dispersion relation enables us to separate the useful signal from the speckle noise. The results for 4 km distance presented in Figure 5b illustrate this fact even more clearly. The signal-to-noise ratio (under *signal* we mean the wave signal placed near the dispersion relation circle, under noise we mean the speckle noise) becomes lower for this case. The wave signal is buried under the noise at the frequencies 0.24295 Hz and 0.25724 Hz while it decreases at other frequencies (that is easily seen in Figure 2b).

The physics of decreasing of the signal-to-noise ratio (SNR) with the distance is in the worsening of the space resolution of nautical radars with the distance. In the first order approximation, neglecting the influence of the radar antenna rotation speed and the variance of the orbital velocity of the

long waves the coefficients $C$, $a$, and $b$ in the formula (10) for the speckle noise $S_n(\mathbf{k})$ have the following form [*Kanevsky,* 2004]

$$C_n \sim (\Delta x \Delta y)^3 \quad (11)$$
$$a = \Delta x^2/8 \quad (12)$$
$$b = \Delta y^2/8 \quad (13)$$

So the spectrum of the speckle noise is proportional to the cube of the radial and tangent resolutions. Also it is seen that the ratio of the main axes of the bell-shaped Gauss function is determined by the corresponding radial and tangent resolutions.

According to the same work the spectrum of the useful signal from the sea waves $S_w(\mathbf{k})$ is proportional to the square of the radial resolution $\Delta x$ and the square of the tangent resolution $\Delta y$:

$$S_w(\mathbf{k}) = C_w \exp\left(-ak_x^2 - bk_y^2\right) \quad (14)$$

$$C_w \sim (\Delta x \Delta y)^2 \quad (15)$$

So, taking into account that the tangent resolution $\Delta y$ is proportional to the angular resolution $\delta_y$ and the distance $R$ from the radar

$$\Delta y = \delta_y R \quad (16)$$

the signal-to-noise ratio $S_{\mathrm{SNR}}(\mathbf{k}) \equiv S_w/S_n$ decreases with worsening of the angle resolution $\delta_y$ and with increasing of the distance $R$:

$$S_{\mathrm{SNR}}(\mathbf{k}) \sim \frac{1}{\delta_y R}. \quad (17)$$

The last formula replies to both questions: a) why the spatial spectra $F_3(k_x, k_y) = S_w + S_n$ looks worse in Figure 5b for 4 km distance than that in Figure 5a for 1 km distance; b) why the level of the speckle noise is higher than that cited in the work [*Nieto Borge et al.,* 2006] so the signal coming from the sea surface waves becomes relatively hard to distinguish on the radar images of the radars with bad angular resolution.

### Angle Resolution and Velocity Vector

The angle resolution of the radar has also another aspect on the possibility of usage of the radar data. The possibilities of evaluation of the directional spectrum of the sea waves and, so, the velocity vector of the surface currents are bonded to the radar angular resolution closely. The maximal values of the radial and tangent wavenumbers $k_x$ and $k_y$ are determined, of cause, by the radial and angle resolution of the radar respectively

$$k_{x,\max} = 2\pi/\Delta x \quad (18)$$

$$k_{y,\max} = 2\pi/(\delta_y R) \quad (19)$$

The radial resolution equals 12 m for the radar pulse 80 ns so $k_{x,\max} = 0.52$ rad m$^{-1}$. While the maximal resolved tangent wavenumber $k_{y,\max}$ consists of 0.19 rad m$^{-1}$ for the radar angular resolution $\delta_y = 1.9^\circ$ and the distance $R = 1000$ m. These limits for the tangent wavenumber $k_{y,\max}$ are shown by the two-sided arrow and vertical lines in Figure 2a. For the distance 4 km the limit for $k_{y,\,max}$ equals 0.047 rad m$^{-1}$ that is shown also Figure 2b. The tangent radar resolution $\Delta y$ for the distances 1 km and 4 km are 33 m and 132 m respectively. So, the waves traveling toward or outward the radar can be detected by the radar only.

It is evident from this analysis that the real spatial spectrum of the sea waves could not be resolved using radars with a wide antenna aperture at large distances (here we mean distances greater than 1 km). The signal spectra shown in Figure 2a, b are some narrowed projections of the real wave spectra. In the case of distance 4 km in Figure 2b it is simply the projection of the real spectrum on the radial direction. In such conditions the directional coefficient $\cos\alpha$ in the dispersion relation (3) can not be used for determination of the current direction so the radial component of the current can be revealed at such situation.

## Conclusions

The analysis of the nautical X-band radar images received using the antenna angle resolution 1.9° showed the possibility to apply the low-cost radars for measuring the field of the radial component of the current velocity up to 4 km from the radar. The radial velocity fields can be interpreted using some assumptions or a priori information about the character of the dynamics in the coastal zone to deduce the full vector velocity fields. For example, as it was shown, to provide the monitoring of the vortex structures in the coastal zone. The evaluation of the the full vector velocity is possible in the near range closer than 1 km to the radar because it is very sensitive to the radar angular resolution.

The radars with the antenna beamwidth 1.9° do register the distinguished signal from the sea waves but the ratio of the wave signal to the speckle noise is twice worse than that for the case of the radars with 0.9° antenna resolution used in Wamos II and SeaDarQ systems. This fact reduces the maximal operating range of the radar for wave and current measurements, and raises the requirement on the minimal wind speed to obtain the detectable backscatter from the sea ripples. In our case, the data proceeding showed the possibility to use the signal got at the wing speed greater than 3 m s$^{-1}$.

The experiments with the X-band radar equipment will be continued on permanent basis since autumn of 2011 at the Black Sea Field Research Facility of the Southern Branch of P. P. Shirshov Institute of Oceanology. We believe that the further progress in the application of the low-cost radar systems for monitoring the current will be closely related to the further development of the speckle noise analysis. The latter could provide us with the information about some relations of the noise with the sea waves height and current velocities.

**Acknowledgments.** The authors are grateful to Sergey I. Badulin for his recommendations and help in the article compilation. This work was supported by the Research Institute of Long-Range Radiocommunication, the program of the Presidium of RAS "The Fundamental problems of nonlinear dynamics", the research program of RAS "The Fundamental problems of oceanology: physics, geology, biology, ecology".

## References

Groeneweg, J., C. Gautier, C. Swinkels, A. van der Westhuysen, (2011), Application of navigation radar data to analyse spatial current and wave fields in the tidal inlet of Ameland, Waves In Shallow Environments (WISE) 2011 Meeting, Qingdao, China.

Hessner, K., K. Reichert, J. Dittmer, J. C. Nieto Borge, (2003), Ocean Wave Measurements by X-Band Radar: from Spectral Wave Parameters to Single Wave Detection, IFREMER Seminar, 2003, http://www.ifremer.fr/dtmsi/colloques/see/communications/C03.doc.

Kanevsky, M. B., (2004), *Theory of radar image of the ocean surface forming*, Institute of Applied Physics RAS, Nizhnij Novgorod, Russia, 124 pp.

Nieto Borge, J. C., K. Hessner, K. Reichert, (1999), Estimation of the Significant Wave Height With X-Band Nautical Radars, OMAE 99 Proceedings.

Nieto Borge, J. C., G. R. Rodriguez, K. Hessner, P. I. Gonzalez, (2004), Inversion of Marine Radar Images for Surface Wave Analysis, *J. Atmos. Oceanic Technol.*, 21, 1291–1300, doi:10.1175/1520-0426(2004)021<1291:IOMRIF>2.0.CO;2.

Nieto Borge, J. C., P. Jarabo-Amores, D. de la Mata-Moya, F. Lopez-Ferreras, (2006), Estimation of Ocean Wave Heights from Temporal Sequences of X-Band Marine Radar Images, Proceedings of 14th European Signal Processing Conference (EUSIPCO 2006), Florence, Italy, September 4–8.

Reichert, K., K. Hessner, J. C. Nieto Borge, J. Dittmer, (1999), WaMos II: A Radar Based Wave and Current Monitoring System, ISOPE 99 Proceedings, Brest 1999, *3*.

Vogelzang, J., J. Vogelzang, K. Boogaard, K. Reichert, K. Hessner, (2000), Wave Height Measurements with Navigation Radar, International Archives of Photogrammetry and Remote Sensing, Vol. XXXIII, Part B7, Amsterdam 2000.

Zatsepin, A. G., V. I. Baranov, A. A. Kondrashov, A. O. Korzh, V. V. Kremenetskii, A. G. Ostrovskii, D. M. Solov'ev, (2011), Sub-mesoscale Vortices on the Caucasus Shelf of the Black Sea and Driven Mechanisms, *Oceanology*, *51*, 4, 581–766.

---

A. I. Azarov, Southern Branch of the P. P. Shirshov Institute of Oceanology, Russian Academy of Science, Gelendzhik, Krasnodar Region, Russia.

V. V. Bakhanov, A. V. Ermoshkin, Institute of Applied Physics, Russian Academy of Science, Nizhnij Novgorod, Russia.

D. V. Ivonin, P. P. Shirshov Institute of Oceanology RAS, 36, Nakhimovsky av., 117997, Moscow, Russia. (toulon@bk.ru)

V. A. Telegin, Research Institute of Long-Range Radiocommunication, Moscow, Russia.